

# SCIENTIFIC REPORTS



OPEN

## Control of Radiative Exciton Recombination by Charge Transfer Induced Surface Dipoles in MoS<sub>2</sub> and WS<sub>2</sub> Monolayers

Received: 15 November 2015

Accepted: 21 March 2016

Published: 07 April 2016

Peng Hu<sup>1</sup>, Jun Ye<sup>2</sup>, Xuexia He<sup>1</sup>, Kezhao Du<sup>1</sup>, Keke K. Zhang<sup>1</sup>, Xingzhi Wang<sup>3</sup>, Qihua Xiong<sup>3</sup>, Zheng Liu<sup>1</sup>, Hui Jiang<sup>1</sup> & Christian Kloc<sup>1</sup>

Due to the two dimensional confinement of electrons in a monolayer of 2D materials, the properties of monolayer can be controlled by electrical field formed on the monolayer surface. F<sub>4</sub>TCNQ was evaporated on MoS<sub>2</sub> and WS<sub>2</sub> monolayer forming dipoles between strong acceptor, F<sub>4</sub>TCNQ, and monolayers of MoS<sub>2</sub> or WS<sub>2</sub>. The strong acceptor attracts electrons (charge transfer) and decreases the number of the ionized excitons. Free excitons undergo radiative recombination in both MoS<sub>2</sub> and WS<sub>2</sub>. Moreover, the photoluminescence enhancement is stronger in WS<sub>2</sub> where the exciton-phonon coupling is weaker. The theoretical model indicates that the surface dipole controls the radiative exciton recombination and enhances photoluminescence radiation. Deposition of F<sub>4</sub>TCNQ on the 2D monolayers enables a convenient control of the radiative exciton recombination and leads to the applications of these materials in lasers or LEDs.

When an exciton, a quasiparticle consisting of an electron and a hole bound together by simple Coulomb interaction, recombines, i) photoluminescence occurs in the case of weak exciton-phonon coupling or ii) exciton recombines radiation-less increasing the phonon energy if this coupling is strong. In a monolayer of transition metal dichalcogenides (TMD), or a two dimensional electron gas, excitons can interact with free electrons forming charged excitons also known as trions, quasiparticles composed of two electrons and a hole<sup>1</sup>. Due to the presence of these tightly bound negative trions, the number of non-bounded excitons available for radiative recombination is limited and the photoluminescence is suppressed. In other words, the non-bounded excitons cannot radiative recombine producing photon (light) because they are bonded with free electrons forming trions<sup>2-6</sup>. Therefore, to increase the photoluminescence, the concentration of trions needs to be reduced. A strong electrical field formed by gate electrode on the two-dimensional (2D) layer of TMD or dipoles on the surface of TMD monolayer can reduce the trion concentration<sup>1</sup>.

In previous studies, a chemical doping method was used to enhance the photoluminescence by interaction of TMD monolayer with acceptor in solvent<sup>2,5</sup>. Furthermore, some reports studied PL and optical properties controlled by the charge transfer between MoS<sub>2</sub> and metal nanoparticle<sup>7</sup> or graphene quantum dots<sup>8</sup>. It was shown that not only the PL intensity has been changed, but also the phase transition in MoS<sub>2</sub> monolayer is caused by charge transfer<sup>9</sup>. In this work, we evaporate 2,3,5,6-tetrafluoro-7,7,8,8-tetracyanoquinodimethane (F<sub>4</sub>TCNQ) on TMD monolayer forming dipoles between strong acceptor, F<sub>4</sub>TCNQ and monolayers of MoS<sub>2</sub> or WS<sub>2</sub>. The strong acceptor attracts electrons (charge transfer) and decreases the number of the ionized excitons. Free excitons undergo radiative recombination in both MoS<sub>2</sub> and WS<sub>2</sub>. Moreover, the photoluminescence enhancement is stronger in WS<sub>2</sub> where the exciton-phonon coupling is weaker. No solvent was used, which provide a clean system to compare to theoretical calculations. The theoretical model indicates that the surface dipole is controlling the radiative exciton recombination, which further increases the photoluminescence.

<sup>1</sup>School of Materials Science and Engineering, Nanyang Technological University, 639798 Singapore. <sup>2</sup>Institute of High Performance Computing, Agency for Science, Technology and Research, 138632 Singapore. <sup>3</sup>School of Physical and Mathematical Sciences, Nanyang Technological University, 637371 Singapore. Correspondence and requests for materials should be addressed to Z.L. (email: z.liu@ntu.edu.sg) or H.J. (email: jianghui@ntu.edu.sg) or C.K. (email: ckloc@ntu.edu.sg)

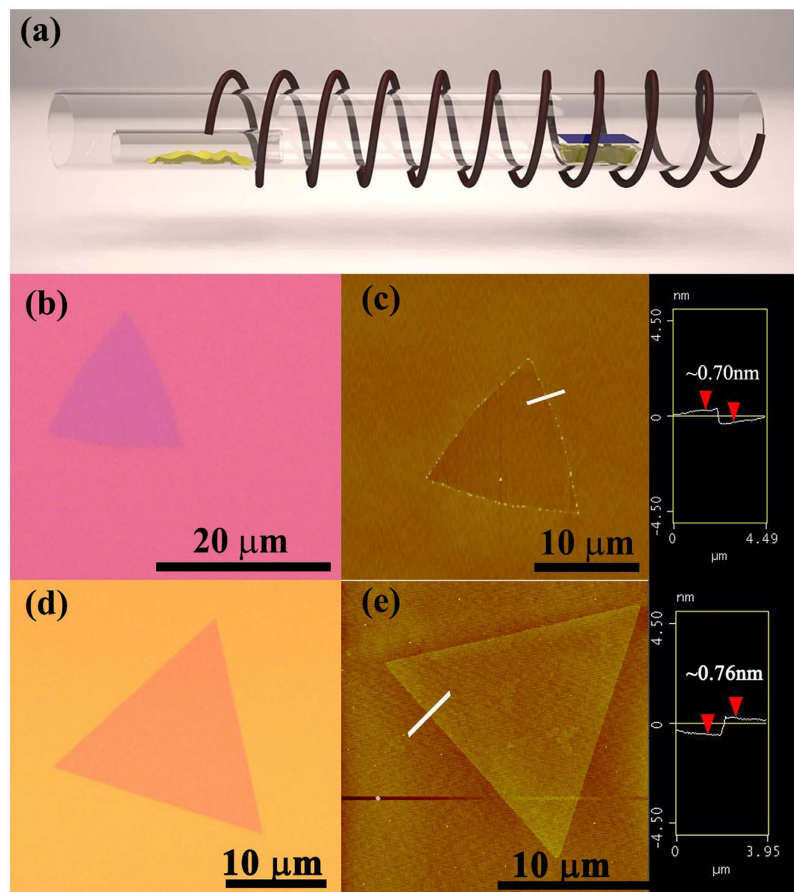


**Figure 1.** (a) Monolayer WS<sub>2</sub> and MoS<sub>2</sub> growth apparatus. (b) Optical image of triangle monolayer WS<sub>2</sub>. (c) AFM image of a monolayer WS<sub>2</sub> on a SiO<sub>2</sub>/Si substrate and the corresponding section analysis. (d) Optical image of triangle monolayer MoS<sub>2</sub>. (e) AFM image of a monolayer MoS<sub>2</sub> on a SiO<sub>2</sub>/Si substrate and the corresponding section analysis.

## Results

**MoS<sub>2</sub> and WS<sub>2</sub> monolayer growth and characterization.** A triangle monolayer of WS<sub>2</sub> and MoS<sub>2</sub> was grown with the chemical vapor deposition (CVD) method onto a SiO<sub>2</sub>/Si wafer. The monolayer growth apparatus is shown in Fig. 1(a). Triangular WS<sub>2</sub> and MoS<sub>2</sub> were grown at random locations on the substrate. Figure 1(b,d) show the optical images of the WS<sub>2</sub> and MoS<sub>2</sub>, respectively. The thickness of the WS<sub>2</sub> and MoS<sub>2</sub> was determined by atomic force microscopy (AFM), as shown in Fig. 1(c,e). The AFM images indicate that both the WS<sub>2</sub> and MoS<sub>2</sub> have a smooth surface. The cross section height of the WS<sub>2</sub> and MoS<sub>2</sub> is approximately 0.70 nm and 0.76 nm, respectively, which corresponds to the monolayers of WS<sub>2</sub><sup>5,10</sup> and MoS<sub>2</sub><sup>11–14</sup>.

The monolayer structure of WS<sub>2</sub> and MoS<sub>2</sub> is further confirmed by the Raman spectrum shown in Fig. 2. The E<sub>2g</sub><sup>1</sup> and A<sub>1g</sub> modes of monolayer WS<sub>2</sub> are located at approximately 355 and 417 cm<sup>-1</sup>, respectively<sup>15–18</sup>. With the number of layers increased, the in-plane vibrational E<sub>2g</sub><sup>1</sup> is slightly red-shifted, and the out-of-plane A<sub>1g</sub> mode is blue-shifted. The energy difference between the Raman E<sub>2g</sub><sup>1</sup> and A<sub>1g</sub> modes increased with the layer number. Thus, the energy difference can be used to identify the number of layers of WS<sub>2</sub>. The energy difference shown in Fig. 2(a) is 62.5 cm<sup>-1</sup>, which coincides with previous reports for monolayer WS<sub>2</sub><sup>15,19</sup>. The same phenomenon is also observed in monolayer MoS<sub>2</sub>. The in-plane vibrational E<sub>2g</sub><sup>1</sup> phonon mode is ~385 cm<sup>-1</sup>, and the out-of-plane A<sub>1g</sub> mode is ~404 cm<sup>-1</sup>. The energy difference between the two modes is also dependent on the number of layers of MoS<sub>2</sub>. The energy difference between the two modes is 18.2 cm<sup>-1</sup>, as shown in Fig. 2(b), indicating that the MoS<sub>2</sub> is a monolayer<sup>2,14,17,20,21</sup>.

### Photoluminescence intensity after F<sub>4</sub>TCNQ was deposited onto monolayer MoS<sub>2</sub>/WS<sub>2</sub>.

Figure 3(a) shows that the PL intensity before and after F<sub>4</sub>TCNQ was deposited onto monolayer WS<sub>2</sub>. The PL intensity is approximately fifty times higher after the F<sub>4</sub>TCNQ deposition. The position of the PL peak of monolayer WS<sub>2</sub> is slightly blue-shifted, while the peak shape did not change, as shown in Fig. 3(b). The PL intensity is also increased by approximately ten times after the F<sub>4</sub>TCNQ is deposited on MoS<sub>2</sub> monolayer. The position of the peak is also slightly blue-shifted, but the shape is not changed, as is shown in Fig. 3(c,d).

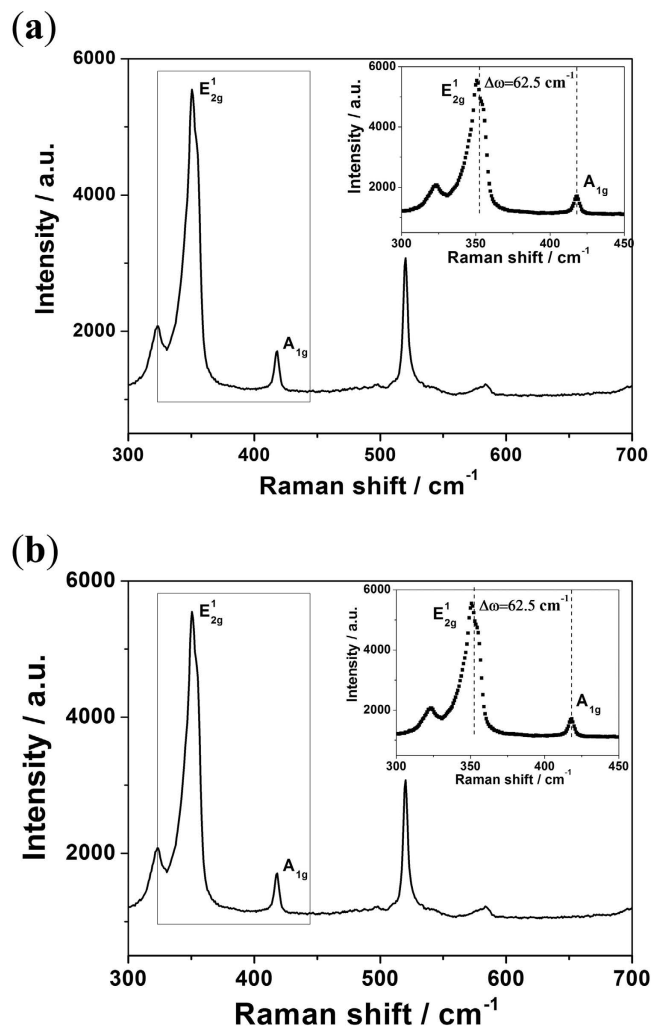


**Figure 2.** Raman spectra of a CVD-grown WS<sub>2</sub> monolayer (a) and MoS<sub>2</sub> monolayer (b). The inset shows the energy difference between the Raman E<sub>2g</sub><sup>1</sup> and A<sub>1g</sub> modes.

## Discussion

To understand the charge transfer from MoS<sub>2</sub>/WS<sub>2</sub> to F<sub>4</sub>TCNQ, we performed density functional (DFT) calculations<sup>22</sup> on the model systems shown in Fig. 4. In both the F<sub>4</sub>TCNQ-doped MoS<sub>2</sub> and WS<sub>2</sub> cases, electron density depletion (as indicated by the white isosurfaces) were found in the interface regions where the nitrogen atoms in the F<sub>4</sub>TCNQ molecules are closest to the surface sulfur atoms in MoS<sub>2</sub> and WS<sub>2</sub>, as shown in Fig. 4(a,c), respectively. The electron density depletion in the MoS<sub>2</sub> layer is slightly greater than that in the WS<sub>2</sub> layer according to the electron density difference plots. An electron density increase (red isosurfaces) is observed on the F<sub>4</sub>TCNQ molecules in both cases, as shown in Fig. 4(a,c). Charge transfer occurs around the interface regions in both cases. The energy level of F<sub>4</sub>TCNQ and MoS<sub>2</sub>/WS<sub>2</sub> are shown in Supporting Information - Figure S1. In addition, the barycenters of the holes (white isosurfaces) shown in Fig. 4(b,d) clearly suggest that the holes are close to the MoS<sub>2</sub> and WS<sub>2</sub> surfaces, indicating the charge transfer from MoS<sub>2</sub> or WS<sub>2</sub> to F<sub>4</sub>TCNQ. The charge transfer distance ( $D_{CT}$ ) between MoS<sub>2</sub> and F<sub>4</sub>TCNQ (calculated  $D_{CT} = 1.299 \text{ \AA}$ ) is shorter than that between WS<sub>2</sub> and F<sub>4</sub>TCNQ (calculated  $D_{CT} = 1.391 \text{ \AA}$ ). However the charge transfer direction, indicated by arrows on the Fig. 4(b,d) is determined by the orientation of F<sub>4</sub>TCNQ molecule relative to the surface of the TMD monolayer.

According to our discussion in introduction, the charge transfer between MoS<sub>2</sub> or WS<sub>2</sub> monolayer and acceptor, F<sub>4</sub>TCNQ forms dipole layers at interface and reduces the ratio of charged exciton to neutral excitons. Therefore, the photoluminescence (PL) of both materials was enhanced due to the charge transfer.

The experimental results for PL enhancement for both MoS<sub>2</sub> and WS<sub>2</sub> are similar to the earlier reported photoluminescence of MoS<sub>2</sub> and WS<sub>2</sub> doped with F<sub>4</sub>TCNQ from solution<sup>2,5</sup>. In previous studies<sup>2,5</sup>, mechanical exfoliated MoS<sub>2</sub> and WS<sub>2</sub> were used. Mechanical exfoliation is the easiest and the fastest method to obtain monolayers of MoS<sub>2</sub> and WS<sub>2</sub>. However, only a small portion of MoS<sub>2</sub> and WS<sub>2</sub> crystals are exfoliate to monolayers, leaving a majority of samples as thicker flakes. In this study, we used the chemical vapor deposition to obtain large-area, high-quality monolayers of MoS<sub>2</sub> and WS<sub>2</sub>. Therefore, after the F<sub>4</sub>TCNQ deposition, our photoluminescence intensity of WS<sub>2</sub> and MoS<sub>2</sub> is approximately fifty times and ten times higher, respectively. Compared to

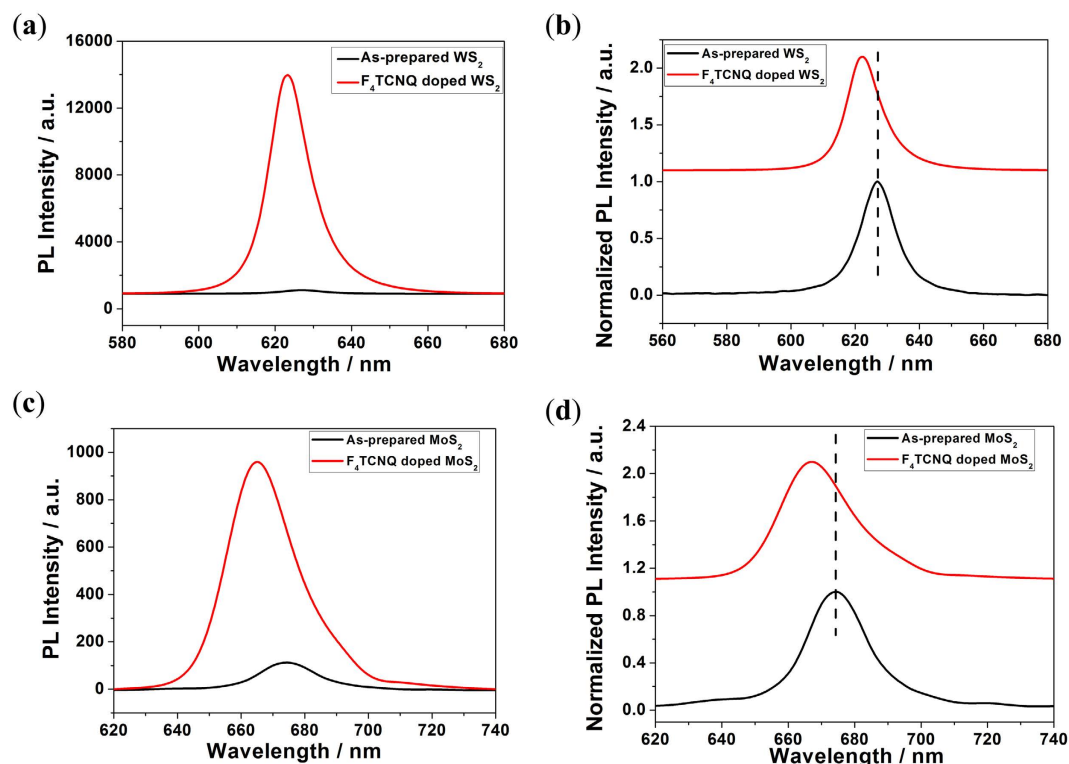


**Figure 3.** PL spectra of monolayer WS<sub>2</sub> (a) and monolayer MoS<sub>2</sub> (c) before and after F<sub>4</sub>TCNQ doping. PL peak shift of monolayer WS<sub>2</sub> (b) and monolayer MoS<sub>2</sub> (d) before and after F<sub>4</sub>TCNQ doping.

the solution-based chemical doping on MoS<sub>2</sub> monolayer<sup>2</sup>, the PL increases approximately three times. During the vacuum deposition of F<sub>4</sub>TCNQ on MoS<sub>2</sub> monolayer, there is no solvent contamination and interaction between MoS<sub>2</sub> and F<sub>4</sub>TCNQ and therefore the PL increases stronger.

The optical properties of MoS<sub>2</sub> and WS<sub>2</sub>, especially the photoluminescence, are affected by the number of layers<sup>6,23</sup>. Few-layered MoS<sub>2</sub> and WS<sub>2</sub> have an indirect band gap and show low photoluminescence, while monolayers of MoS<sub>2</sub> and WS<sub>2</sub> have a direct bandgap and strong photoluminescence<sup>23,24</sup>. To understand the effects of charge transfer, the photoluminescence peaks, which are due to the direct band gap transition, have been analyzed by fitting them with photoluminescence from trions and photoluminescence from neutral excitons represented by two Lorentzian functions, as shown in Fig. 5. For the all cases studied, the photoluminescence signal can be decomposed as A and B peaks, but the intensity of the B peak is negligible. The A peak can be further decomposed to trion (X<sup>-</sup>) and exciton (X) components. Peak positions from the fitting can be found in Table 1. The exciton binding energy of MoS<sub>2</sub> and WS<sub>2</sub> (1.85 eV and 1.985 eV) was determined in our work. The trion spectral weight  $I_{X^-}/I_{total}$  was also calculated and listed in Table 1.

For both WS<sub>2</sub> and MoS<sub>2</sub>, the trion spectral weight  $I_{X^-}/I_{total}$  decreases after charge transfer, as shown in Table 1. This indicates that the charge transfer significantly decreases the concentration of trions by transferring electrons from the trions into acceptors, thereby enhancing the photoluminescence.

Upon the deposition of F<sub>4</sub>TCNQ on the monolayers, the charge transfer reaches a maximum because the trion spectral weight reaches the saturation region at approximately 0.2. We observe that the peaks for the corresponding X<sup>-</sup> and X of PL are sharper for WS<sub>2</sub> than for MoS<sub>2</sub>. The wider peak width is associated with a stronger coupling strength or a larger Huang-Rhys factor *S* for a typical semiconductor<sup>25,26</sup>, so that we may ascribe the narrower PL peaks for WS<sub>2</sub> samples compared to MoS<sub>2</sub> as indicative of slightly weaker exciton-phonon coupling<sup>27</sup>. After charge transfer to the F<sub>4</sub>TCNQ molecules, the peak width change is almost the same. The weaker exciton-phonon scattering of WS<sub>2</sub> results in narrower PL peaks with a larger amplitude.

The DFT calculated electron transferred from MoS<sub>2</sub> and WS<sub>2</sub> to F<sub>4</sub>TCNQ was 0.271 and 0.237, respectively. These data are in good agreement with the trion spectral weight data (Table 1). Larger amount of charge transferred causes more trions to be dissociated to excitons, thereby leading to a lower trion spectral weight. The surface dipole is formed due to the charge transferred from MoS<sub>2</sub>/WS<sub>2</sub> to F<sub>4</sub>TCNQ. The amount of transferred charge can control the intensity and position of PL. The adding electrons to or withdrawing electrons from the 2D monolayer decreases<sup>7-9</sup> or increases (this work) the intensity of PL.

It is worth to notice that a dipoles formed by charge transfer to acceptor deposited directly on 2D semiconductor is comparable to dipoles formed by Helmholtz double layer in an electrolyte double layer transistor (EDLT), where gate is a reference electrode in an ionic organic liquid. In an EDLT, the number of induced charges in the transistor channel is in the range of 10<sup>14</sup> 1/cm<sup>2</sup>. It is almost one order of magnitude larger than the charge induced by the layer of dipoles in our experiment, but two orders of magnitude larger than the charge induced

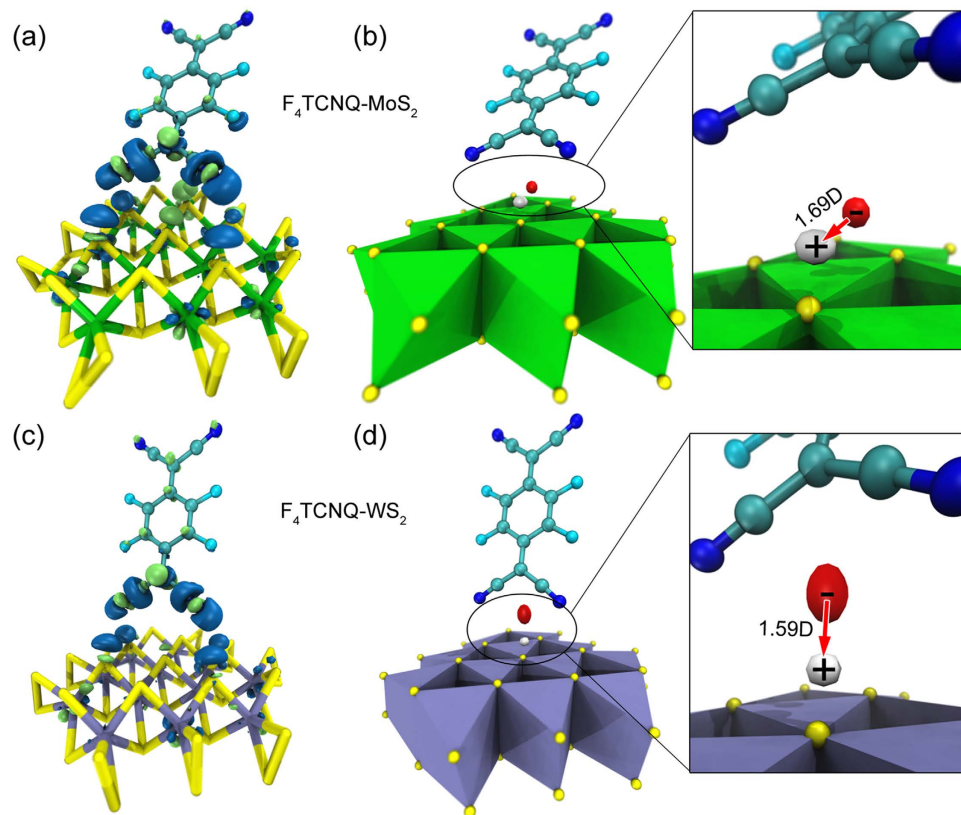


**Figure 4.** (a) Electron density differences (with  $\pm$  isovalues of 0.005 a.u.) and (b) barycenters (with  $\pm$  isovalues of 0.0001 a.u.) of an  $F_4TCNQ$ -doped  $MoS_2$  cluster model. Electron density differences (with  $\pm$  isovalues of 0.005 a.u.) and barycenters (with  $\pm$  isovalues of 0.0001 a.u.) for  $F_4TCNQ$ -doped  $WS_2$  cluster model are given in (c,d), respectively. Green and blue isosurfaces indicate positive and negative values in electron density differences, while red and white isosurfaces indicate plus (electron density increase) and minus (electron density depletion) values of barycenters in (b,d). The dipole moment variation before and after charge transfer are also displayed in the enlarged view of (c,d), with  $\pm$  sign indicating virtual charge of the barycenters due to electron density depletion/increase.

in  $MoS_2$  transistor with 280 nm  $SiO_2$  and gate voltage of  $-70 V^1$ . Such high concentration of charge induced in a monolayer of TMD semiconductors should lead to correlated effects like ferromagnetism or to superconductivity in EDLT  $MoS_2$  system<sup>28</sup>. Additionally acceptor layer deposited on the surface on 2D semiconductors can be considered as a stable gate that doesn't required additional connector for gate voltage.

## Conclusion

In summary, triangle monolayer  $WS_2$  and  $MoS_2$  were grown using the chemical vapor deposition (CVD) method. The formation of the monolayers was confirmed by both AFM and Raman spectra. The PL increased after a thin layer of  $F_4TCNQ$  was deposited on the surface of the  $WS_2$  and  $MoS_2$  monolayers. The ratio of charged excitons, trions, to neutral excitons decreases due to the charge transfer from monolayer  $WS_2$  and  $MoS_2$  to strong acceptor,  $F_4TCNQ$ . The weaker exciton-phonon interaction of  $WS_2$  results in narrower PL peaks with larger amplitudes than in  $MoS_2$  where this interaction is strong. Acceptors or donators deposited on the surface of  $MoS_2$  or  $WS_2$  and also on other 2D monolayers provides an effective mechanism for controlling the electron distribution in such heterojunctions. In this way, it is a convenient method of tuning the optoelectronic properties of 2D materials and leads to the application of these materials in lasers or LEDs.

## Methods

**Chemicals and materials.**  $WO_3$  (>99.5%),  $MoO_3$  (>99.5%) and sulfur (>99.95%) powders were purchased from Sigma-Aldrich and used without any purification.  $F_4TCNQ$  (>99.5%) was purchased from Jilin OLED Materials Tech. Co. Ltd. and purified at 220 °C via physical vapor transport (PVT).

**Preparation of  $MoS_2$  and  $WS_2$  monolayers.** For both the triangular shaped  $MoS_2$  and  $WS_2$  monolayers, we used the same method of chemical vapor deposition (CVD). The growth process for the two materials is almost the same, with the only difference being the precursor. Commercially available  $SiO_2/Si$  substrates were used in this study. All the substrates were successively cleaned with acetone, methanol,  $H_2O_2/H_2SO_4$  (1 volume/4 volume) and distilled water in an ultrasonic bath for 5 min and then dried in ambient  $N_2$ . First, fine  $WO_3$  or  $MoO_3$  powder was spread on the bottom of the crucible. One piece of  $SiO_2/Si$  substrate (1 × 1 cm) was

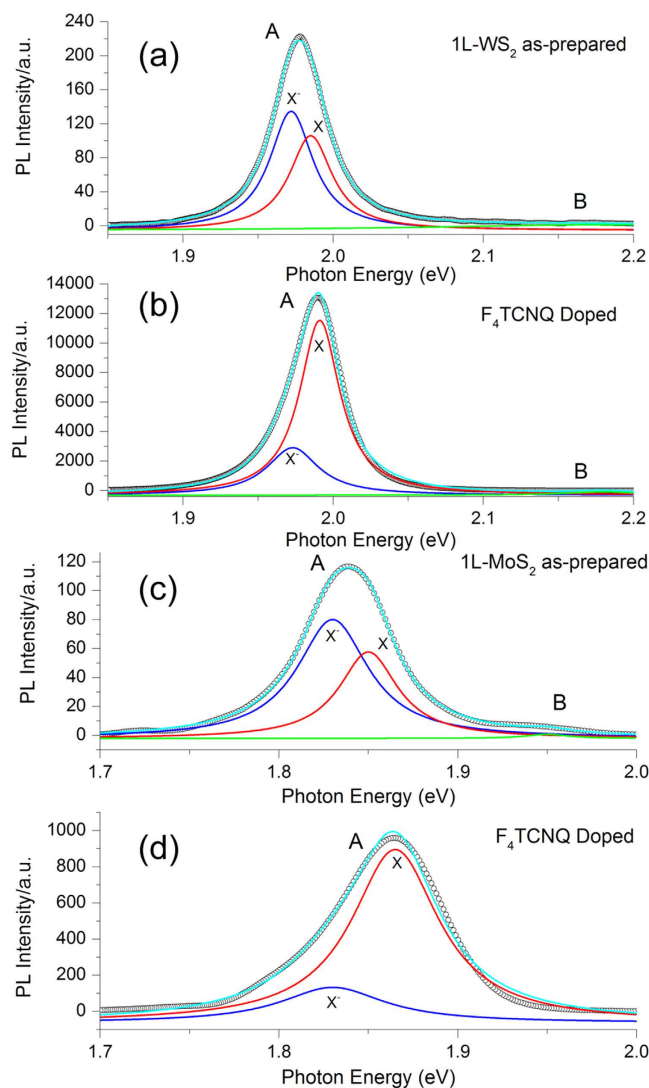


**Figure 5.** Fitted PL spectra of monolayer WS<sub>2</sub> (a) before and (b) after F<sub>4</sub>TCNQ doping. Fitted PL spectra of monolayer MoS<sub>2</sub> (c) before and after F<sub>4</sub>TCNQ doping (d). Lorentzian functions were used to fit the A and B peaks, with A peaks assumed to be composed of trions (X<sup>-</sup>) and excitons (X).

Sample	Peak name	Peak Position (eV)	FWHM(meV)	$I_{X^-}/I_{total}$
1 L WS <sub>2</sub> as-prepared	X <sup>-</sup> trion	1.972 (1.96)	35	0.63
	X exciton	1.985	35	
F <sub>4</sub> TCNQ doped 1 L WS <sub>2</sub>	X <sup>-</sup> trion	1.973 (1.98)	42	0.25
	X exciton	1.991 (2.02)	33	
1 L MoS <sub>2</sub> as-prepared	X <sup>-</sup> trion	1.83 (1.84)	48	0.70
	X exciton	1.85 (1.88)	40	
F <sub>4</sub> TCNQ doped 1 L MoS <sub>2</sub>	X <sup>-</sup> trion	1.83 (1.84)	70	0.20
	X exciton	1.865 (1.88)	60	

**Table 1.** Peak position and width for Lorentzian functions used to fit PL peak A in Fig. 5. (The values in brackets for peak positions were previously reported<sup>2,5</sup>).

placed face-down on the crucible, and the crucible was put in the center of the growth furnace. Another small crucible with approximately 50 mg sulfur powder was put in another part of the furnace near the gas input side at a temperature of 200 °C. The furnace was heated to 750 °C at 25 °C/min and then maintained at that temperature for 20 min before naturally being cooled down to room temperature. Argon gas was provided during the whole growth process at 60 sccm.

**Preparation of F<sub>4</sub>TCNQ layers on WS<sub>2</sub> and MoS<sub>2</sub> monolayers.** 2-nm F<sub>4</sub>TCNQ was deposited on the WS<sub>2</sub> and MoS<sub>2</sub> monolayers by the evaporation of F<sub>4</sub>TCNQ in a Tectra mini-coater (Germany) with a deposition rate of 0.1 angstrom per second.

**Characterization.** Photoluminescence was measured at the same area before and after F<sub>4</sub>TCNQ deposition. Both the laser beams (solid-state laser, 473 nm and Nd:YAG solid-state laser, 532 nm) were collimated and focused through a ×100 objective onto the sample surface. All the spectra were collected using a confocal triple-grating spectrometer (Horiba-JY T64000). Raman spectra were recorded using a Renishaw Raman microscope configured with a charge-coupled device array detector with the excitation laser line of 532 nm. Atomic force microscopy was performed on a Digital Instruments 3100.

**Density functional theory calculations.** The geometry of the F<sub>4</sub>TCNQ on the surface of the MoS<sub>2</sub>/WS<sub>2</sub> was optimized using the DMol<sup>3</sup><sup>29,30</sup> with the dispersion-corrected (OBS) PW91 (GGA) functional at the level of the DNP basis set. The geometry of the models is regarded as converged when the total energy difference is less than  $1 \times 10^{-5}$  Ha, the total force difference is less than  $4 \times 10^{-3}$  Ha/Å, and the maximum displacement of atoms is less than  $5 \times 10^{-3}$  Å during the optimization. The optimized geometries of the models were subsequently fed into the ORCA 3.0.3 package<sup>31</sup> to perform single-point energy calculations (with SCF convergence criteria set as  $1 \times 10^{-6}$  Ha) at the level of B3LYP/6-31G(d,p) (with Mo and W atoms treated using SDD effective core potentials<sup>32</sup>). To facilitate the charge transfer analysis, the MultiWFN 3.3.7 package<sup>33</sup> was used to calculate the charge transfer based on electron density difference.

## References

- Mak, K. F. *et al.* Tightly bound trions in monolayer MoS<sub>2</sub>. *Nat. Mater.* **12**, 207–211 (2013).
- Mouri, S., Miyauchi, Y. & Matsuda, K. Tunable Photoluminescence of Monolayer MoS<sub>2</sub> via Chemical Doping. *Nano Lett.* **13**, 5944–5948 (2013).
- Newaz, A. K. M. *et al.* Electrical control of optical properties of monolayer MoS<sub>2</sub>. *Solid State Commun.* **155**, 49–52 (2013).
- Tongay, S. *et al.* Broad-Range Modulation of Light Emission in Two-Dimensional Semiconductors by Molecular Physisorption Gating. *Nano Lett.* **13**, 2831–2836 (2013).
- Peimyoo, N. *et al.* Chemically Driven Tunable Light Emission of Charged and Neutral Excitons in Monolayer WS<sub>2</sub>. *ACS Nano* **8**, 11320–11329 (2014).
- Dhall, R. *et al.* Direct Bandgap Transition in Many-Layer MoS<sub>2</sub> by Plasma-Induced Layer Decoupling. *Adv. Mater.* **27**, 1573–1578 (2015).
- Li, Z. *et al.* Active Light Control of the MoS<sub>2</sub> Monolayer Exciton Binding Energy. *ACS Nano* **9**, 10158–10164 (2015).
- Li, Z. *et al.* Graphene Quantum Dots Doping of MoS<sub>2</sub> Monolayers. *Adv. Mater.* **27**, 5235–5240 (2015).
- Kang, Y. *et al.* Plasmonic Hot Electron Induced Structural Phase Transition in a MoS<sub>2</sub> Monolayer. *Adv. Mater.* **26**, 6467–6471 (2014).
- Peimyoo, N. *et al.* Nonblinking, Intense Two-Dimensional Light Emitter: Monolayer WS<sub>2</sub> Triangles. *ACS Nano* **7**, 10985–10994 (2013).
- Salehzadeh, O., Tran, N. H., Liu, X., Shih, I. & Mi, Z. Exciton Kinetics, Quantum Efficiency, and Efficiency Droop of Monolayer MoS<sub>2</sub> Light-Emitting Devices. *Nano Lett.* **14**, 4125–4130 (2014).
- Lee, Y.-H. *et al.* Synthesis of Large-Area MoS<sub>2</sub> Atomic Layers with Chemical Vapor Deposition. *Adv. Mater.* **24**, 2320–2325 (2012).
- Zhan, Y., Liu, Z., Najmaei, S., Ajayan, P. M. & Lou, J. Large-Area Vapor-Phase Growth and Characterization of MoS<sub>2</sub> Atomic Layers on a SiO<sub>2</sub> Substrate. *Small* **8**, 966–971 (2012).
- Najmaei, S. *et al.* Vapour phase growth and grain boundary structure of molybdenum disulphide atomic layers. *Nat. Mater.* **12**, 754–759 (2013).
- Zhang, Y. *et al.* Controlled Growth of High-Quality Monolayer WS<sub>2</sub> Layers on Sapphire and Imaging Its Grain Boundary. *ACS Nano* **7**, 8963–8971 (2013).
- Berkdemir, A. *et al.* Identification of individual and few layers of WS<sub>2</sub> using Raman Spectroscopy. *Sci. Rep.* **3**, 1755 (2013).
- Huo, N. *et al.* Interlayer coupling and optoelectronic properties of ultrathin two-dimensional heterostructures based on graphene, MoS<sub>2</sub> and WS<sub>2</sub>. *J. Mater. Chem. C* **3**, 5467–5473 (2015).
- Wang, X. H. *et al.* Photoluminescence and Raman mapping characterization of WS<sub>2</sub> monolayers prepared using top-down and bottom-up methods. *J. Mater. Chem. C* **3**, 2589–2592 (2015).
- Gutiérrez, H. R. *et al.* Extraordinary Room-Temperature Photoluminescence in Triangular WS<sub>2</sub> Monolayers. *Nano Lett.* **13**, 3447–3454 (2013).
- Zhang, W. *et al.* High-Gain Phototransistors Based on a CVD MoS<sub>2</sub> Monolayer. *Adv. Mater.* **25**, 3456–3461 (2013).
- Nan, H. *et al.* Strong Photoluminescence Enhancement of MoS<sub>2</sub> through Defect Engineering and Oxygen Bonding. *ACS Nano* **8**, 5738–5745 (2014).
- Le Bahers, T., Adamo, C. & Ciofini, I. A Qualitative Index of Spatial Extent in Charge-Transfer Excitations. *J. Chem. Theory Comput.* **7**, 2498–2506 (2011).
- Mak, K. F., Lee, C., Hone, J., Shan, J. & Heinz, T. F. Atomically Thin MoS<sub>2</sub>: A New Direct-Gap Semiconductor. *Phys. Rev. Lett.* **105**, 136805 (2010).
- Splendiani, A. *et al.* Emerging Photoluminescence in Monolayer MoS<sub>2</sub>. *Nano Lett.* **10**, 1271–1275 (2010).
- Chakraborty, B. *et al.* Symmetry-dependent phonon renormalization in monolayer MoS<sub>2</sub> transistor. *Phys. Rev. B* **85**, 161403 (2012).
- Ye, J., Zhao, Y., Ng, N. & Cao, J. Width of Phonon Sidebands in the Brownian Oscillator Model. *J. Phys. Chem. B* **113**, 5897–5904 (2009).
- Ho, C. H., Wu, C. S., Huang, Y. S., Liao, P. C. & Tiong, K. K. Temperature dependence of energies and broadening parameters of the band-edge excitons of Mo<sub>1-x</sub>W<sub>x</sub>S<sub>2</sub> single crystals. *J. Phys. Condens. Matter* **10**, 9317–9328 (1998).
- Ye, J. T. *et al.* Superconducting Dome in a Gate-Tuned Band Insulator. *Science* **338**, 1193–1196 (2012).
- Delley, B. An all-electron numerical method for solving the local density functional for polyatomic molecules. *J. Chem. Phys.* **92**, 508–517 (1990).
- Delley, B. From molecules to solids with the DMol<sup>3</sup> approach. *J. Chem. Phys.* **113**, 7756–7764 (2000).
- Neese, F. The ORCA program system. *Wiley Interdiscip. Rev. Comput. Mol. Sci.* **2**, 73–78 (2012).
- Andrae, D., Häußermann, U., Dolg, M., Stoll, H. & Preuß, H. Energy-adjusted ab initio pseudopotentials for the second and third row transition elements. *Theoret. Chim. Acta* **77**, 123–141 (1990).
- Lu, T. & Chen, F. Multiwfn: A multifunctional wavefunction analyzer. *J. Comput. Chem.* **33**, 580–592 (2012).

## Acknowledgements

This research was conducted by the NTU-HUJ-BGU Nanomaterials for Energy and Water Management Programme under the Campus for Research Excellence and Technological Enterprise (CREATE), which is supported by the National Research Foundation, Prime Minister's Office, Singapore. Z.L. thanks Singapore National Research Foundation for NRF RF Award No. NRF-RF2013-08 and the start-up funding from Nanyang Technological University (M4081137.070). Q.X. and C.K. gratefully thanks Singapore Ministry of Education for the strong support via an AcRF tier2 grant (MOE2012-T2-2-086) and AcRT RG125/4 grant. J.Y. would like to thank the support from the Institute of High Performance Computing, Agency for Science, Technology and Research, Singapore.

## Author Contributions

P.H., X.H., H.J., Z.L. and C.K. conceived the experiments. P.H. and X.H. performed the experiments including monolayers growth, characterization and data analysis. K.D., K.K.Z., X.W. and Q.X. performed the PL measurement. J.Y. performed all theoretical calculations and wrote respective discussions. J.Y. also prepared Fig. 4 and assist fitting of Fig. 5 and preparation of Table 1. P.H., X.H., H.J. and C.K. co-wrote the manuscript. Z.L., H.J. and C.K. supervised the project. All of the authors reviewed the manuscript, discussed the data and gave profound suggestions.

## Additional Information

**Supplementary information** accompanies this paper at <http://www.nature.com/srep>

**Competing financial interests:** The authors declare no competing financial interests.

**How to cite this article:** Hu, P. *et al.* Control of Radiative Exciton Recombination by Charge Transfer Induced Surface Dipoles in MoS<sub>2</sub> and WS<sub>2</sub> Monolayers. *Sci. Rep.* **6**, 24105; doi: 10.1038/srep24105 (2016).



This work is licensed under a Creative Commons Attribution 4.0 International License. The images or other third party material in this article are included in the article's Creative Commons license, unless indicated otherwise in the credit line; if the material is not included under the Creative Commons license, users will need to obtain permission from the license holder to reproduce the material. To view a copy of this license, visit <http://creativecommons.org/licenses/by/4.0/>



# SCIENTIFIC REPORTS

**OPEN**

## **Corrigendum: Control of Radiative Exciton Recombination by Charge Transfer Induced Surface Dipoles in MoS<sub>2</sub> and WS<sub>2</sub> Monolayers**

Peng Hu, Jun Ye, Xuexia He, Kezhao Du, Keke K. Zhang, Xingzhi Wang, Qihua Xiong, Zheng Liu, Hui Jiang & Christian Kloc

Correction to: *Scientific Reports* <https://doi.org/10.1038/srep24105>; published online 07 April 2016; updated 05 April 2018

This article contains an error in Figure 2, where the same image was inadvertently shown in both panel (a) and (b). The correct Figure 2 appears below:

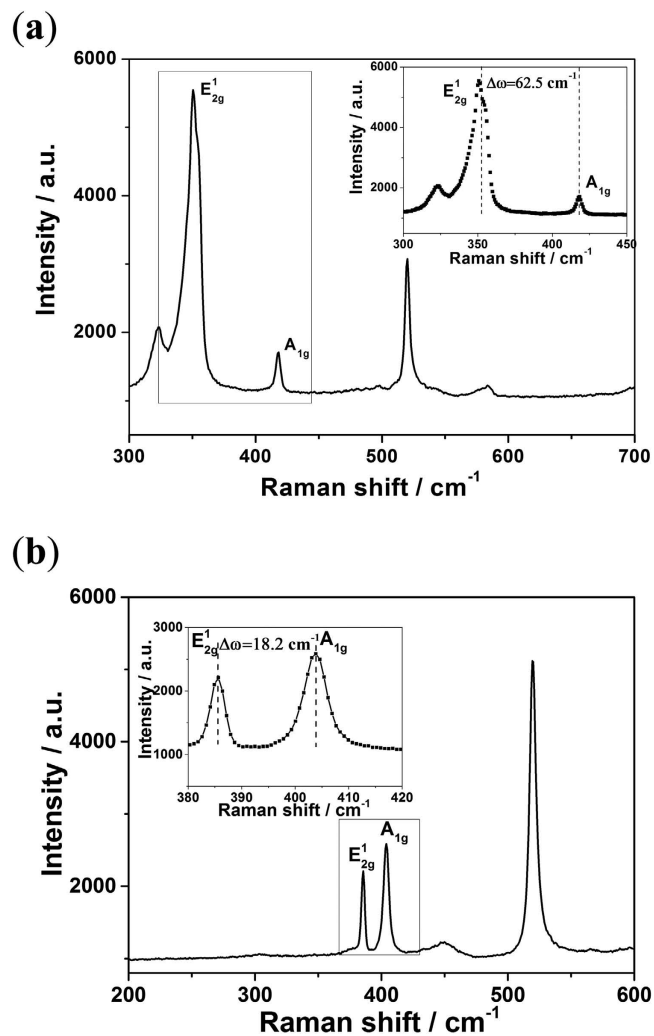


Figure 2.



This work is licensed under a Creative Commons Attribution 4.0 International License. The images or other third party material in this article are included in the article's Creative Commons license, unless indicated otherwise in the credit line; if the material is not included under the Creative Commons license, users will need to obtain permission from the license holder to reproduce the material. To view a copy of this license, visit <http://creativecommons.org/licenses/by/4.0/>

© The Author(s) 2018